**The Fourth IEEE RAS/EMBS International Conference on Biomedical Robotics and Biomechatronics Roma, Italy. June 24-27, 2012**

# Model Based Control of Series Elastic Actuators

Markus Grün, Roman Müller and Ulrich Konigorski

***Abstract*— This contribution presents a comprehensible model based approach of a control structure to control the output force of series elastic actuators. The controller is based on a linear model of the actuator, which can be reduced to a $PT_2$ element if a disturbance compensator is included. This allows for a straightforward design of a state space controller and an intuitive choice of the controller parameters. An actuator design is presented and the required system parameters are identified. The performance of the control structure is proven by experiment.**

## I. INTRODUCTION

In classic engineering applications high output impedance of actuators has always been desired to facilitate an accurate position control. This implies a stiff actuator that is robust against disturbances, such as external forces or friction. Compliance in the power transmission has always been considered as a disturbance and been tried to eliminate by design or control.

However, many applications in the biomedical field, such as exoskeletons, rehabilitation- and assistive robots rather require an accurate force control, low output impedance, back-driveability, and shock resistance. These are demands that cannot be met with classic stiff actuators. Series elastic actuators (SEA's) provide these functionalities by intentionally placing a compliant element between the motor and the load.

The spring between the motor and the load fulfills two functions: First, it decouples the dynamics of the motor, including intertia, friction, and disturbances, from the load and vice versa, isolating the drive train from shocks introduced by the load. Second, it can be used as a torque sensor by multiplying the measured spring deflection with the spring stiffness, turning the force control problem into a position control problem.

Many designs [1]–[6] and controllers [6]–[10] have been presented for series elastic actuators and the system behaviour in the open and closed loop conditions were analyzed, as well as the impact of the compliance in regard to the controller and the overall performance [11]. The following example will give a brief insight into the advantages of including compliance into the drive train in terms of force control.

The authors gratefully thank the Deutsche Forschungsgemeinschaft (DFG) for funding this work by the project with the reference number KO 1876/12-1

M. Grün and U. Konigorski are with the Department of Control Engineering and Mechatronics, Technische Universität Darmstadt, 64283 Darmstadt, Germany. mgruen@iat.tu-darmstadt.de, u.konigorski@iat.tu-darmstadt.de

R. Müller is with the Institute of Electromechanical Design, Technische Universität Darmstadt, 64283 Darmstadt, Germany. r.mueller@emk.tu-darmstadt.de

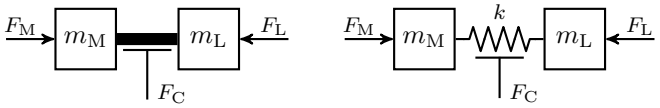


Fig. 1. *Left:* rigid coupling, *right:* compliant coupling between motor $m_\mathrm{M}$ and load $m_\mathrm{L}$

### A. Importance of Elasticity

Series elastic actuators are often used in exoskeletons and active orthoses to support the user during challenging tasks. If no force support is desired, e.g. during the swing phase in gait, the force between actuator and limb should be zero; otherwise the natural motion would be impeded. This means the closed loop system has to provide a zero torque output, even during motion. A typical geared electric motor, though, has a significant mechanical resistance in unpowered condition due to friction and inertia, multiplied by the square of the gear ratio. The following simple example shows the necessity of elasticity between motor and load in order to provide a zero torque output.

Two scenarios are considered whereby all parameters are transferred to the translational domain. First, the motor is connected to the human limb by a rigid link, as depicted in Fig. 1.

The coupling force $F_\mathrm{C}$ between the motor mass $m_\mathrm{M}$ and the load mass $m_\mathrm{L}$ is measured by a force sensor of infinite stiffness. The motor force $F_\mathrm{M}$ acts on the motor mass and the load force $F_\mathrm{L}$ acts on the load mass. The coupling force can be derived by the following equation

$$F_\mathrm{C}(s) = \underbrace{\frac{m_\mathrm{L}}{m_\mathrm{M}+m_\mathrm{L}}}_{G_w(s)} F_\mathrm{M}(s) + \underbrace{\frac{m_\mathrm{M}}{m_\mathrm{M}+m_\mathrm{L}}}_{G_z(s)} F_\mathrm{L}(s). \quad (1)$$

The first term describes the control transfer function $G_w(s)$ and the second term describes the disturbance transfer function $G_z(s)$.

If the control loop is closed by an arbitrary controller $R(s)$, $F_\mathrm{M}(s) = -R(s)\,F_\mathrm{C}(s)$, the closed loop disturbance transfer function becomes

$$G_{\mathrm{z,\,closed}}(s) = \frac{F_\mathrm{C}(s)}{F_\mathrm{L}(s)} = \frac{m_\mathrm{M}}{m_\mathrm{M}+m_\mathrm{L}+R(s)m_\mathrm{L}}. \quad (2)$$

In order not to feel a resistance if a movement is initiated, the closed loop disturbance transfer function must not have a direct feedthrough. That means

$$\lim_{s\to\infty} G_{\mathrm{z,\,closed}}(s) \stackrel{!}{=} 0. \quad (3)$$

**978-1-4577-1200-5/12/$26.00 ©2012 IEEE**

One can clearly see that with any regular controller

$$R(s) = K\frac{a_m s^m + \cdots + a_1 s + 1}{b_n s^n + \cdots + b_1 s + 1} \quad \text{with} \quad n \geq m \qquad (4)$$

this goal can not be achieved unless the controller gain $K$ is infinite.

Since the closed loop transfer function has a direct feedthrough regardless of the chosen controller, the user would feel a resistive force $F_\mathrm{C}$ immediatly when initiating a movement by tightening the muscle, i.e. applying a force $F_\mathrm{L}$.

If the two masses are coupled by an elastic element with a spring coefficient $k$, the coupling force $F_\mathrm{C}$ becomes

$$F_\mathrm{C}(s) = \frac{m_\mathrm{L}}{\frac{m_\mathrm{M} m_\mathrm{L}}{k} s^2 + m_\mathrm{M} + m_\mathrm{L}} F_\mathrm{M}(s) + \ldots$$
$$\ldots + \frac{m_\mathrm{M}}{\frac{m_\mathrm{M} m_\mathrm{L}}{k} s^2 + m_\mathrm{M} + m_\mathrm{L}} F_\mathrm{L}(s) \qquad (5)$$

and the closed loop disturbance transfer function is

$$G_{\mathrm{z,\,closed}}(s) = \frac{m_\mathrm{M}}{\frac{m_\mathrm{M} m_\mathrm{L}}{k} s^2 + m_\mathrm{M} + m_\mathrm{L} + R(s) m_\mathrm{L}}. \qquad (6)$$

Due to the elastic element $k$, the direct feedthrough of the closed loop transfer function is eliminated and any regular controller $R(s)$ can achieve the goal defined above and therefore enable the implementation of several control objectives such as back-driveability and impedance control.

### *B. Controller for Series Elastic Actuators*

Several control structures have been proposed in the literature for controlling the output force or impedance of series elastic actuators. Almost all of them are based on linear control theory and are rather simple, using only basic PD- or PID controllers.

Pratt and Williamson [7] proposed a modified PID force controller with additional feedforward terms to compensate motor inertia. Passivity, and thus stability during interaction with passive loads is guaranteed by proper selection of the feedforward terms and replacement of the integrator with a low pass filter, thus disabling the ability to compensate static errors. Later, Pratt also proposed a cascaded impedance controller [8], based on a PID position controller in the inner loop and feedforward terms for compensation of motor inertia.

Vallery [9] investigated several cascaded control structures with a velocity controller in the inner loop in terms of passivity to ensure stability in human interacting devices. Sensinger [10] also proposed an impedance controller, based on a simple proportional controller in the inner loop, and Wyeth [1] investigated the closed loop behaviour of a SEA with a cascaded controller, using a PI velocity controller in the inner loop and a PI torque controller in the outer loop.

By far the most advanced controller was proposed by Kong [6] and uses a PD force controller which is enhanced by a disturbance observer to compensate for modelling errors and plant variations. This control structure can be reformulated into an *internal model control* structure.

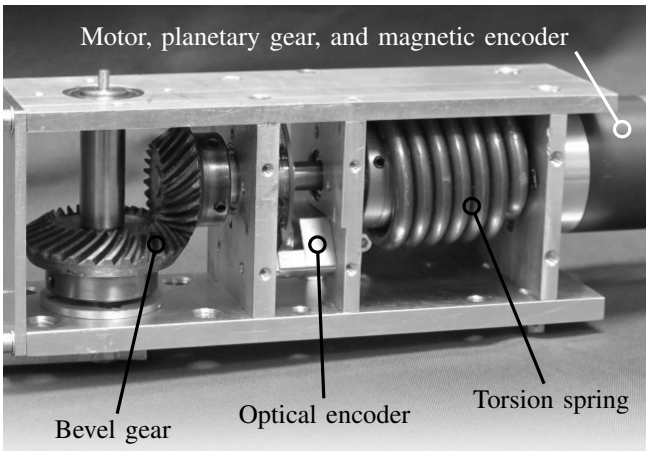


Fig. 2. Actuator setup

## II. MECHANICAL DESIGN

The presented actuator is inspired by the design proposed by Kong [6]. It consists of a motor, a planetary gear box, a torsion spring, and two encoders to measure the load and motor angles. Furthermore, a bevel gear is used for $90°$ torque redirection to allow attachment to a knee orthosis. The setup is depicted in Fig. 2. The requirements for the selection of the main components are based on preliminary measurements and gait analysis [12], [13]. Basically, there are two aspects which have to be considered during the development of the SEA:

First of all, the actuator has to provide the required support torque. We have defined that up to $30\,\%$ of the maximum knee torque during the sit-to-stand (STS) movement should be supported. Preliminary measurements of the knee torque during the STS movement revealed a maximum knee torque of $(1.07 \pm 0.12)\,\mathrm{N\,m/kg}$ [13]. Based on these preliminary measurements and the body weight of the subject ($75\,\mathrm{kg}$), the maximum torque that the actuator must provide is about $27\,\mathrm{N\,m}$. Furthermore, gait analysis measurements indicated $2\,\mathrm{W/kg}$ of maximum mechanical power in the knee joint during STS. On the condition that $30\,\%$ of mechanical power should be supported, a mechanical peak output of about about $45\,\mathrm{W}$ is expected.

The second aspect concerns the dynamics of the components. The actuator must be capable of providing the desired torque within a given time and follow the load angle up to a defined velocity. The bending angle is about $110°$ and the sit-to-stand process takes about $2\,\mathrm{s}$.

The actuator is depicted in Fig. 2 and consists of the components described in table I. The setup has a mass of about $1.4\,\mathrm{kg}$ and contains a lateral mechanical connection to the orthosis. The dimensions of the setup are $270\,\mathrm{mm} \times 60\,\mathrm{mm} \times 45\,\mathrm{mm}$.

## III. MODELLING AND IDENTIFICATION

Series elastic actuators only consist of a geared motor and a spring, mounted on the output shaft. It is assumed that the motor can be operated in a current controlled mode and that

TABLE I
COMPONENTS OF THE SERIES ELASTIC ACTUATOR

| Component | Type and manufacturer | Remarks |
|---|---|---|
| Motor | 3257 DC motor, Faulhaber (Schönaich, Germany) | Max. torque 70 mNm |
| Gear | 38A planetary gear, Faulhaber | Gear ratio $p = 1/60$ |
| Motor Encoder | IE3-512 incremental magnetic encoder, Faulhaber | 512 lines per rev. |
| Motor Controller | MCDC 3006 S/C motion controller, Faulhaber | Operated in current controlled mode |
| Load Encoder | AEAS-7000 optical absolute encoder, Agilent | 12 bit resolution |
| Torsion spring | Custom design, Febrotec (Halver, Germany) | $k = 0.21\,\mathrm{N\,m/^\circ}$ |
| Bevel gear | spiral toothed bevel gear (Mädler, Germany) | Gear ratio $q = 2/3$ |

the gear is ideal and the spring $k$ and damping $d$ are linear. With these assumptions the block diagram of the SEA can easily be determined as seen in Fig. 3.

Only the motor constant $c_\mathrm{M}$, the gear ratios $p$ and $q$, and the spring coefficient $k$ are known from datasheets. Since the proposed control algorithm is based on this model of the SEA, the damping coefficient $d$ and the motor inertia $J$ have to be identified.

### A. Identification of Damping Coefficient $d$

For the identification of motor inertia and damping coefficient, the spring is detached from the motor. The system therefore only consists of the motor and the gear and the equation of motion is

$$J\ddot{\varphi}_\mathrm{M}(t) = c_\mathrm{M}\, i(t) - M_\mathrm{D}(t). \tag{7}$$

For identifying the damping torque $M_\mathrm{D}$, the motor is driven by a constant current $i(t) = I$. The motor accelerates and reaches a final velocity $\dot{\varphi}_\infty$ that depends only on the current $I$ and the damping torque $M_\mathrm{D}$.

Fig. 4 shows the measured final velocities plotted against the current. Contrary to expectations, the measured values do not follow the Stribeck curve with a significant static friction. No stiction is present at all; even at very low currents the motor moves and three almost linear areas can be identified. As this is contrary to expectations, it is presumed that the motor controller has some kind of compensation built in. However, as the motor and controller form a unit and are

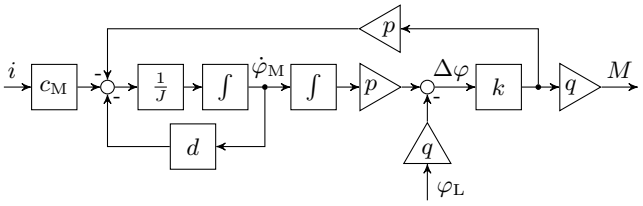


Fig. 3. Block diagram of the series elastic actuator

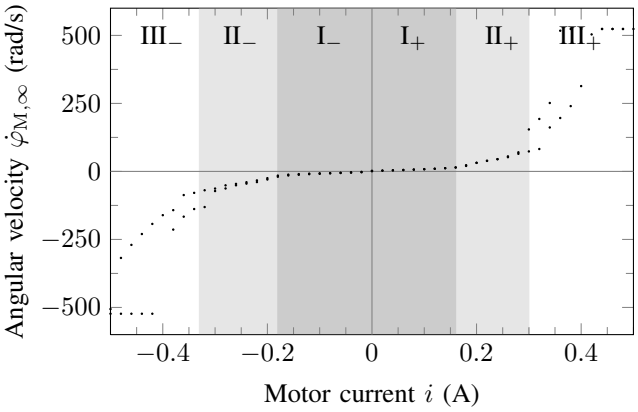


Fig. 4. Measured angular velocities $\dot{\varphi}_{\mathrm{M},\infty}$ over motor current $i$

used together in the SEA, these are the values that apply to the system.

To obtain a linear coefficient $d$ for the damping, a regression line is fitted to the values in the second area of the measured velocities as it is assumed that the motor will be operated mainly at these velocities. This yields to a damping coefficient of

$$d = 83.7 \times 10^{-6}\,\frac{\mathrm{N\,m\,s}}{\mathrm{rad}}$$

and equation (7) can now be formulated as:

$$J\ddot{\varphi}_\mathrm{M}(t) = c_\mathrm{M}\, i(t) - d\,\dot{\varphi}_\mathrm{M}(t). \tag{8}$$

### B. Identification of Motor Inertia $J$

The motor inertia is identified in a similar way. Equation (8) describes a first order system

$$\frac{\dot{\varphi}_\mathrm{M}(s)}{i(s)} = \frac{c_\mathrm{M}}{Js + d} = \frac{K}{Ts + 1} \tag{9}$$

with $K = c_\mathrm{M}/d$ and $T = J/d$. The time constant $T$ can be obtained by the step response of the system (9). Since $d$ is not constant over the whole current range as seen in Fig. 4, but linear within an area, start- and end value of the step have to be in the same area in order to keep (8) linear and therefore (9) existent.

Ten step responses each in ascending and descending direction were recorded and the time constants $T$ determined

TABLE II
IDENTIFIED MOTOR INERTIA

| area | motor inertia | area | motor inertia |
|---|---|---|---|
| $\mathrm{I}^{\uparrow}_{-}$ | $62.8 \times 10^{-7}\,\mathrm{kgm^2}$ | $\mathrm{I}^{\downarrow}_{-}$ | $62.8 \times 10^{-7}\,\mathrm{kgm^2}$ |
| $\mathrm{I}^{\uparrow}_{+}$ | $53.4 \times 10^{-7}\,\mathrm{kgm^2}$ | $\mathrm{I}^{\downarrow}_{+}$ | $49.7 \times 10^{-7}\,\mathrm{kgm^2}$ |
| $\mathrm{II}^{\uparrow}_{-}$ | $67.9 \times 10^{-7}\,\mathrm{kgm^2}$ | $\mathrm{II}^{\downarrow}_{-}$ | $33.7 \times 10^{-7}\,\mathrm{kgm^2}$ |
| $\mathrm{II}^{\uparrow}_{+}$ | $85.7 \times 10^{-7}\,\mathrm{kgm^2}$ | $\mathrm{II}^{\downarrow}_{+}$ | $41.9 \times 10^{-7}\,\mathrm{kgm^2}$ |
| $\mathrm{III}^{\uparrow}_{-}$ | $62.7 \times 10^{-7}\,\mathrm{kgm^2}$ | $\mathrm{III}^{\downarrow}_{-}$ | $71.6 \times 10^{-7}\,\mathrm{kgm^2}$ |
| $\mathrm{III}^{\uparrow}_{+}$ | $67.6 \times 10^{-7}\,\mathrm{kgm^2}$ | $\mathrm{III}^{\downarrow}_{+}$ | $57.6 \times 10^{-7}\,\mathrm{kgm^2}$ |
| Mean: $59.8 \times 10^{-7}\,\mathrm{kgm^2}$ | | | |

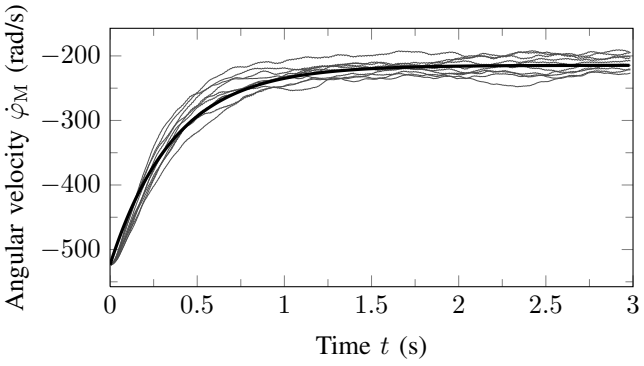


Fig. 5. Measured step responses and fitted $\mathrm{PT}_1$ element in area $\mathrm{III}_-^{\downarrow}$

by taking the time $T_{95}$ where 95 % of the final value is reached: $T = 1/3\,T_{95}$. The motor inertia can then be determined by

$$J = c_\mathrm{M}\frac{T_{95}}{3}\frac{\Delta i}{\Delta\dot{\varphi}}. \tag{10}$$

The determined values for the motor inertia within the different areas can be found in table II. The indices "+" and "−" denote the corresponding areas in the positive and negative plane, and the superscripts "↑" and "↓" the direction of the step, respectively. Fig. 5 exemplarily depicts the step response of a $\mathrm{PT}_1$ element with the corresponding time coefficient $T$ over the measured step responses.

## IV. CONTROLLER DESIGN

The gear ratios $p$ and $q$ are omitted in this section for the sake of simplicity. The block diagram depicted in Fig. 3 can be transformed into the block diagram highlighted gray in Fig. 6, that shows the classic $\mathrm{PT}_2$ structure but with an additional input from the load angle $\varphi_\mathrm{L}$. This input is considered as a disturbance. The control transfer function and disturbance transfer functions are

$$G_\mathrm{w}(s) = \frac{\Delta\varphi(s)}{i(s)} = \frac{c_\mathrm{M}}{Js^2 + ds + k} \tag{11}$$

$$G_\mathrm{z}(s) = \frac{\Delta\varphi(s)}{\varphi_\mathrm{L}(s)} = \frac{k}{Js^2 + ds + k} - 1. \tag{12}$$

Since the load angle and therefore the disturbance is measured, a classic approach by implementing a disturbance compensator $V(s)$ can be applied.

The disturbance $\varphi_\mathrm{L}$ should have no impact on the control output $\Delta\varphi$ and the output torque $M = k\Delta\varphi$, respectively; therefore,

$$0 \stackrel{!}{=} \Big[V(s)G_\mathrm{w}(s) + G_\mathrm{z}(s)\Big]\varphi_\mathrm{L}(s), \tag{13}$$

which yields

$$V(s) = -\frac{G_\mathrm{z}(s)}{G_\mathrm{w}(s)} = -\frac{Js^2 + ds}{c_\mathrm{M}}. \tag{14}$$

As $V(s)$ is not causal, it needs to be extended with a $\mathrm{PT}_2$ element with unity gain and sufficiently small time constant $T_\mathrm{N}$

$$\tilde{V}(s) = -\frac{Js^2 + ds}{c_\mathrm{M}}\frac{1}{(T_\mathrm{N}s + 1)^2}. \tag{15}$$

A similar feedforward term was proposed by Pratt [7] but without damping $d$ and without considering feasibility.

Now the system is approximatly decoupled from the load angle $\varphi_\mathrm{L}$ and describes a simple $\mathrm{PT}_2$ element as in (11). Formulating the state space description yields

$$\begin{aligned}\underbrace{\begin{bmatrix}\dot{\varphi}_\mathrm{M}(t)\\ \ddot{\varphi}_\mathrm{M}(t)\end{bmatrix}}_{\dot{\mathbf{x}}(t)} &= \underbrace{\begin{bmatrix}0 & 1\\ -\frac{k}{J} & -\frac{d}{J}\end{bmatrix}}_{\mathbf{A}}\underbrace{\begin{bmatrix}\varphi_\mathrm{M}(t)\\ \dot{\varphi}_\mathrm{M}(t)\end{bmatrix}}_{\mathbf{x}(t)} + \underbrace{\begin{bmatrix}0\\ \frac{1}{c_\mathrm{M}}\end{bmatrix}}_{\mathbf{B}} i(t)\\ y(t) &= \underbrace{\begin{bmatrix}k & 0\end{bmatrix}}_{\mathbf{C}}\mathbf{x}(t),\end{aligned} \tag{16}$$

and a state space controller with a disturbance observer can now be implemented to control the output torque $M = k\Delta\varphi$ and to compensate for nonlinearities and the incomplete decoupling of the disturbance compensator $\tilde{V}(s)$. These disturbances are summarized in an additional input $z(t)$ to the system

$$\dot{\mathbf{x}}(t) = \mathbf{A}\mathbf{x}(t) + \mathbf{B}i(t) + \mathbf{E}z(t). \tag{17}$$

Since $z(t)$ acts on the control input $\mathbf{E} = \mathbf{B}$, and it is assumed that the disturbance is piecewise constant, $\dot{z}(t) = 0$. Therefore, the extended state space description for the disturbance observer is

$$\begin{aligned}\underbrace{\begin{bmatrix}\dot{\hat{\varphi}}_\mathrm{M}(t)\\ \ddot{\hat{\varphi}}_\mathrm{M}(t)\\ \dot{\hat{z}}(t)\end{bmatrix}}_{\dot{\hat{\mathbf{x}}}_\mathrm{e}(t)} &= \underbrace{\begin{bmatrix}0 & 1 & 0\\ -\frac{k}{J} & -\frac{d}{J} & \frac{1}{J}\\ 0 & 0 & 0\end{bmatrix}}_{\mathbf{A}_\mathrm{e}}\underbrace{\begin{bmatrix}\hat{\varphi}_\mathrm{M}(t)\\ \dot{\hat{\varphi}}_\mathrm{M}(t)\\ \hat{z}(t)\end{bmatrix}}_{\hat{\mathbf{x}}_\mathrm{e}(t)} + \underbrace{\begin{bmatrix}0\\ \frac{1}{c_\mathrm{M}}\\ 0\end{bmatrix}}_{\mathbf{B}_\mathrm{e}} i(t)\\ \hat{y}(t) &= \underbrace{\begin{bmatrix}1 & 0 & 0\end{bmatrix}}_{\mathbf{C}_\mathrm{e}}\hat{\mathbf{x}}_\mathrm{e}(t); \qquad \hat{z}(t) = \underbrace{\begin{bmatrix}0 & 0 & 1\end{bmatrix}}_{\mathbf{C}_\mathrm{z}}\hat{\mathbf{x}}_\mathrm{e}(t)\end{aligned} \tag{18}$$

and the observed states are computed by

$$\dot{\hat{\mathbf{x}}}_\mathrm{e}(t) = \big(\mathbf{A}_\mathrm{e} - \mathbf{L}\mathbf{C}_\mathrm{e}\big)\hat{\mathbf{x}}_\mathrm{e}(t) + \mathbf{B}_\mathrm{e}u(t) + \mathbf{L}y(t), \tag{19}$$

with $\mathbf{L}$ being the observer matrix, which is derived by the well known LQ method with the weighting matrices $\mathbf{Q}$ and $S$ for system noise and measurement noise, respectively.

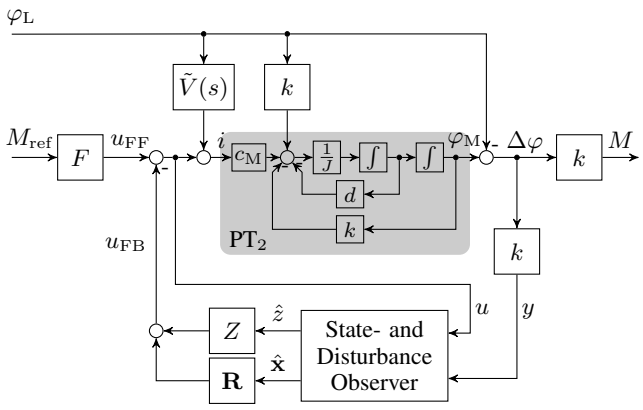


Fig. 6. Overall Control Structure of the proposed controller. *Gray*: Block diagram of SEA, transfomed into $\mathrm{PT}_2$ structure; the gear ratios $p$ and $q$ are omitted for simplicity

The disturbance correction term $Z$ is computed by

$$Z = -(\mathbf{B}^{\mathrm{T}}\mathbf{B})^{-1}\mathbf{B}^{\mathrm{T}}\mathbf{E}. \tag{20}$$

The straightforward modelling and controller design allow for an intuitive choice of the controller gains. First, the time constant $T_{\mathrm{N}}$ of the $\mathrm{PT}_2$ element has to be chosen according to the expected frequency of the input excitation $\varphi_{\mathrm{L}}$. Then, the command input response is set by appropriate selection of the closed loop poles, defining the controller matrix $\mathbf{R}$ and prefilter $F$. Finally, the weighting matrices $\mathbf{Q}$ and $S$ have to be chosen, which determine the observer matrix $\mathbf{L}$. This, however, requires some experiments to find suitable values.

## V. EXPERIMENTAL RESULTS

Precise torque control over a sufficiently large frequency range is the desired objective of series elastic actuators. Especially, keeping the desired torque while the load angle varies is an essential task for actuators used in exoskeletons or active orthoses. This includes providing zero torque at the output shaft, which is necessary during the swing phase of normal gait, for example.

To analyze the performance of the overall control system in Fig. 6, a lever was mounted to the output shaft of the series elastic acutator described in section II in order to excite the load angle $\varphi_{\mathrm{L}}$ by hand.

The performance of the control system is compared to that of a cascaded controller with inner PI-velocity loop and outer PI-torque loop. Two test scenarios are presented in this section, the first one showing the performance of the control system at zero torque and varying load angle, the second one showing the response to a step signal of $5\,\mathrm{Nm}$.

### A. Parameters

With the parameter identified in section III, the disturbance transfer function (12) becomes

$$G_{\mathrm{z}}(s) = \frac{\Delta\varphi(s)}{\varphi_{\mathrm{L}}(s)} = -\frac{s^2 + 14s}{s^2 + 14s + 1.035}. \tag{21}$$

Note that the load angle $\varphi_{\mathrm{L}}$ is taken on the spring side of the bevel gear, therefore the gear ratio $q$ does not appear in the formula.

The poles of the $\mathrm{PT}_2$ element, necessary to make the disturbance compensator (14) causal are set to $-62.83$, enabling a compensation of disturbances with frequencies of up to $10\,\mathrm{Hz}$. $\tilde{V}(s)$ therefore becomes

$$\tilde{V}(s) = \frac{37.57s\ (s+14)}{(s+62.83)^2}. \tag{22}$$

The closed loop poles for the state space controller are placed at $-16$ and $-18$; the weighting matrices $\mathbf{Q}$ and $S$ are set to

$$\mathbf{Q} = \mathrm{diag}\begin{bmatrix}1 & 10 & 5000\end{bmatrix} \quad \text{and} \quad S = 1. \tag{23}$$

### B. Zero Torque Control

For the first test scenario, the reference torque $M_{\mathrm{ref}}$ was set to zero and the load angle $\varphi_{\mathrm{L}}$ was excited by hand. It was attempted to move the load angle similarly to a sine sweep with constant amplitude and increasing frequency. Fig. 7 and Fig. 8 show the output torques $M$, which were computed from the measured load angles and motor angles and the spring coefficient: $M = k(\varphi_{\mathrm{M}} - \varphi_{\mathrm{L}})$.

The measured output torque in Fig. 7 shows an excellent performance of the proposed controller. At low frequencies the output torque is near zero with minor peaks at the direction changes of the load angle. These peaks increase with the frequency of the excitation but stay below $0.5\,\mathrm{Nm}$ and are barely noticeable. These peaks result from the nonlinearities in the drive chain, such as stiction and the nonlinear damping depicted in Fig. 4. Increasing the corresponding element in the weighting matrix $\mathbf{Q}$ reduces the height of the peaks, but also increases noise. A trade-off between low noise motor current and low peaks in the torque has to be found. An appropriate value for this element cannot be found analytically but has to be determined by experiment.

The cascaded controller (Fig. 8) is not capable of providing zero torque while the load angle varies, even though PI-controllers are used in both control loops. The output torque increases with higher frequencies.

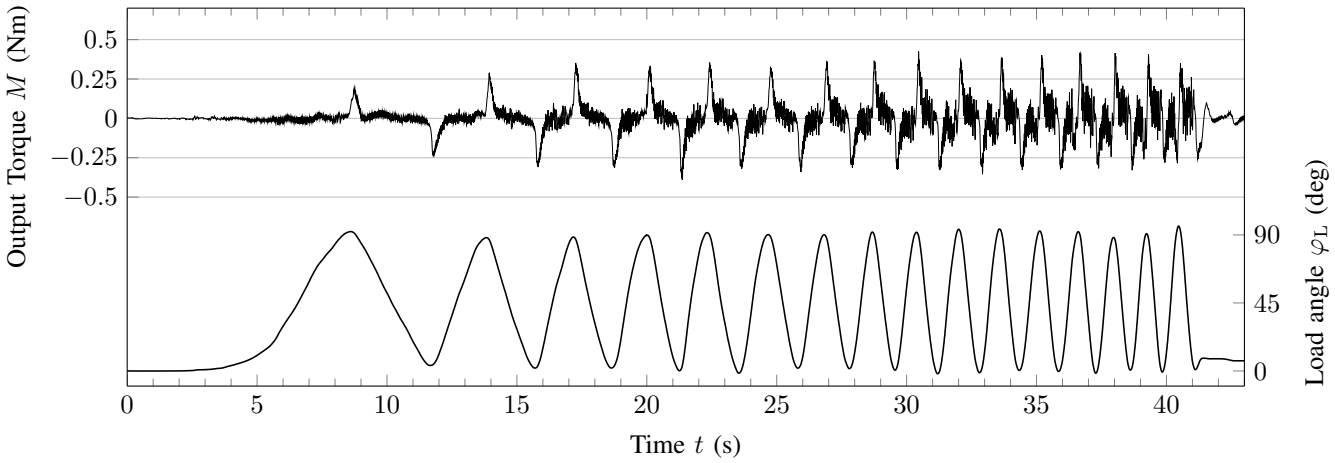


Fig. 7. Proposed controller: zero torque control; the load angle is excited by hand. *Top*: Output torque; *Bottom*: Load angle

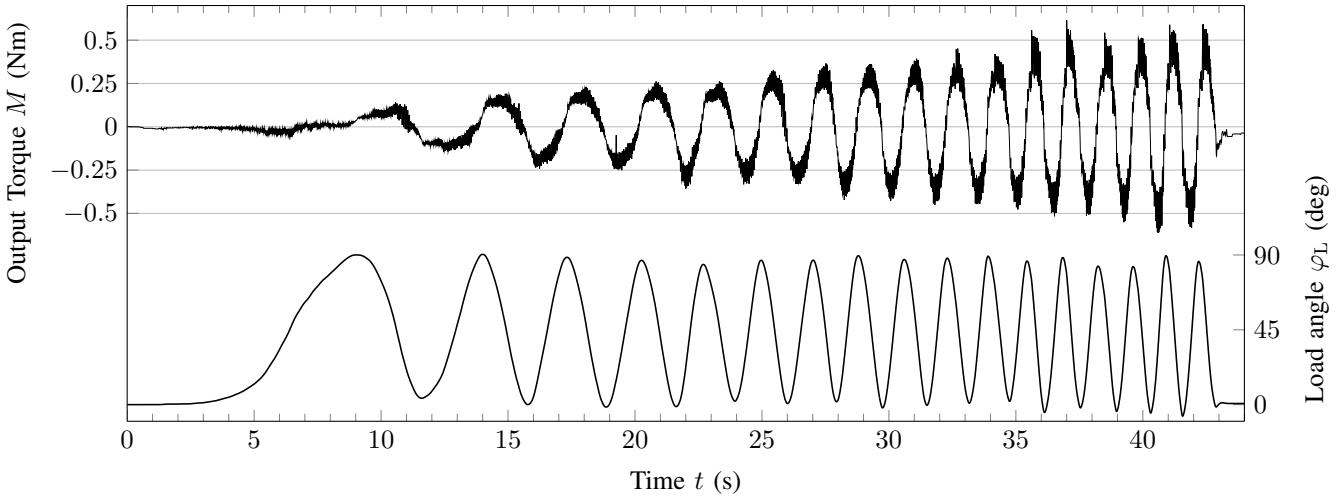


Fig. 8. Cascaded controller: zero torque control; the load angle is excited by hand. *Top*: Output torque; *Bottom*: Load angle

### C. Non-Zero Torque Control

For the second test scenario, the load angle $\varphi_{\mathrm{L}}$ is mechanically locked at $0°$. The reference torque is a step signal with an amplitude of $5\,\mathrm{Nm}$.

As can be seen in Fig. 9 the proposed controller shows an excellent behaviour with minimal overshoot. The settling time is about $0.23\,\mathrm{s}$. The cascaded controller has a settling time of $0.42\,\mathrm{s}$ and the step response oscillates strongly and has an overshoot of $33\,\%$.

## VI. CONCLUSIONS

The proposed control structure is capable of precisely generating the desired torque, independent of the excitation of the load angle. The unknown motor parameters, necessary for the controller design, can be identified by simple experiments without the need of extensive test machinery. The straightforward modelling and controller design allow for a simple and intuitive choice of the appropriate controller parameters to achieve excellent results.

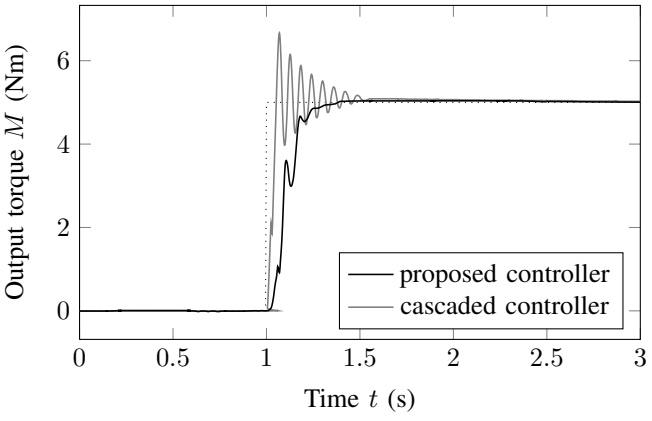


Fig. 9. Step response of the closed loop system; *solid:* output torque; *dotted:* reference torque

## REFERENCES


[1] G. Wyeth, "Control issues for velocity sourced series elastic actuators," in *Proceedings of Australasian Conference on Robotics and Automation 2006 (ACRA 2006)*, 2006.

[2] J. F. Veneman, R. Ekkelenkamp, R. Kruidhof, F. C. Van Der Helm, and H. Van Der Kooij, "A series elastic- and bowden-cable-based actuation system for use as torque actuator in exoskeleton-type robots," *International Journal of Robotic Research*, vol. 25, no. 3, pp. 261–281, March 2006.

[3] E. Torres-Jara and J. Banks, "A simple and scalable force actuator," in *Proceedings of the 35th Int. Symp. on Robotics*, 2004.

[4] J. Pratt, B. Krupp, and C. Morse, "Series elastic actuators for high fidelity force control," *Industrial Robot: An International Journal*, vol. 29, no. 3, pp. 234–241, 2002.

[5] K. Kong and M. Tomizuka, "Flexible joint actuator for patient's rehabilitation device," in *16th IEEE International Symposium on Robot and Human interactive Communication, 2007 (RO-MAN 2007)*, aug. 2007, pp. 1179 –1184.

[6] K. Kong, J. Bae, and M. Tomizuka, "Control of rotary series elastic actuator for ideal force-mode actuation in human-robot interaction applications," *IEEE/ASME Transactions on Mechatronics*, vol. 14, no. 1, pp. 105 –118, feb. 2009.

[7] G. Pratt and M. Williamson, "Series elastic actuators," in *Proceedings of the IEEE/RSJ Int. Conf. on Intelligent Robots and Systems,1995*, vol. 1, aug 1995, pp. 399 –406 vol.1.

[8] G. Pratt, P. Willisson, C. Bolton, and A. Hofman, "Late motor processing in low-impedance robots: impedance control of series-elastic actuators," in *Proceedings of the 2004 American Control Conference, 2004.*, vol. 4, 30 2004-july 2 2004, pp. 3245 –3251 vol.4.

[9] H. Vallery, R. Ekkelenkamp, H. van der Kooij, and M. Buss, "Passive and accurate torque control of series elastic actuators," in *Proceedings of the IEEE/RSJ Int. Conf. on Intelligent Robots and Systems, 2007 (IROS 2007)*, 29 2007-nov. 2 2007, pp. 3534 –3538.

[10] J. W. Sensinger and R. F. Weir, "Unconstrained impedance control using a compact series elastic actuator," in *Proceedings of the 2nd IEEE/ASME Int. Conf. on Mechatronic and Embedded Systems and Applications*, aug. 2006, pp. 1 –6.

[11] D. W. Robinson, "Design and analysis of series elasticity in closed-loop actuator force control," Ph.D. dissertation, Massachusetts institute of Technology (MIT), 2000.

[12] J. Block, M. Vanoncini, and S. Wolf, "3d analysis of sit-to-stand: Reference data for designing a motorized orthosis," in *Proceedings of the 7. Jahrestagung der Deutschen Gesellschaft für Biomechnik*, 2011.

[13] J. Block, M. Vanoncini, D. Heitzmann, M. Alimusaj, R. Müller, P. Pott, H. F. Schlaak, T. Meiss, R. Werthschützky, M. Grün, U. Konigorski, and S. Wolf, "Entwicklung einer aktiven Orthese mit Leistungsabgabe - Erhebung von Referenzdaten, Aufbau und Test der Prototypen am Probanden," in *Proceedings of the ORTHOPÄDIE + REHA-TECHNIK*, 2012.